

## THERMOPHYSICAL PROPERTIES OF MATERIALS

# Molecular Dynamics Simulation of Adsorption of Ozone and Nitrate Ions by Water Clusters

A. E. Galashev

*Institute of Industrial Ecology, Ural Branch, Russian Academy of Sciences, Yekaterinburg, Russia*

Received December 14, 2010

**Abstract**—Coadsorption of ozone molecules and nitrate ions by water clusters was studied by the molecular dynamics technique. The maximum value of an average O–H···O bond length in a water carcass is realized at the minimum specific number of such bonds when the ratio of adsorbed ozone molecules to nitrate ions captured by a cluster is two. IR absorption and reflection spectra were reshaped significantly, and new peaks appeared at Raman spectra due to the addition of ozone and nitrate ions to the disperse water system. After ozone and nitrate ions were captured, the average (in frequency) IR reflection coefficient of the water disperse system increased drastically and the absorption coefficient fell.

DOI: 10.1134/S0018151X12010051

### INTRODUCTION

Nitrate ions are some of the most widespread ions in the Earth's atmosphere. Their proportion exceeds that of atmospheric  $\text{Cl}^-$  ions by more than 3.5 times and, by hundreds of times, that of  $\text{Br}^-$  ions [1, 2]. Many atmospheric processes are explained by their presence. In work [3], solvation of nitrate ions was studied at the air–water interface. A nitrate ion was shown to prefer surface solvation to bulk solvation. The lifetime of  $\text{NO}_3^-$  in the atmosphere depends on irreversible losses of  $\text{N}_2\text{O}_5$ , because thermodynamic equilibrium is established quickly between these two components. Under the assumption that a stationary state is established during the decomposition of  $\text{N}_2\text{O}_5$ , the  $\text{NO}_3^-$  lifetime becomes inversely proportional to the  $\text{NO}_2$  concentration. Recently great attention has been paid to investigation of the destructive effect that  $\text{Cl}^-$  and  $\text{Br}^-$  ions have on the content of atmospheric ozone [2], whereas the effect of interaction between  $\text{NO}_3^-$  ions and ozone at the water surface has been elucidated in only a few works.

Since ozone is a greenhouse gas, its content in the troposphere affects the global climate. Oxidation of trace components is often treated as a self-purifying ability of the atmosphere. Although there is no definition of oxidizing ability, it is often associated with excess of OH. However, many other oxidants, including  $\text{O}_2$  and  $\text{O}_3$ , and free radicals different from OH, can contribute to the oxidation process taking place in the atmosphere. The  $\text{NO}_3^-$  radical is an important atmospheric oxidizer at night. The main mechanisms of  $\text{NO}_3^-$  decomposition are a reaction with organic

components and heterogeneous losses (reactions on the Earth and on the surface of aerosol particles, including those in clouds). The gas-phase reaction between  $\text{NO}_3^-$  and water vapor is endothermic.

Water vapor exerts a paramount influence upon radiation transport in the troposphere. The water-vapor concentration changes noticeably on the height scale  $\sim 1$  km and on the horizontal scale  $\sim 100$  km. According to the authors' estimation, about 18% of the total amount of water vapor is in a state corresponding to the initial condensation stage, i.e., in the form of clusters [4]. At present, no efforts have been undertaken to study the effect that water clusters have on ozone content and activity in the atmosphere. With the current average surface humidity of the Earth of  $11 \text{ g/m}^3$ , the total estimated mass of water clusters in the troposphere is near  $2.08 \times 10^{15} \text{ kg}$ , and the mass of tropospheric ozone is only  $0.15 \times 10^{12} \text{ kg}$ . The mass of water clusters is  $\sim 1380$  times above that of ozone. Taking into account the size distribution of clusters, one can demonstrate that there are about 15 500 typical water clusters for every ozone molecule in the troposphere [4]. Thus, the probability of interaction between water clusters and ozone molecules is quite high. In principle, water clusters can adsorb all tropospheric ozone.

Absorption of ozone, oxygen, nitrogen monoxide and dioxide, and chlorine and bromine ions by atmospheric moisture is investigated in the works [4–9]. There are no data on how the presence of  $\text{NO}_3^-$  ions can change ozone absorption by water clusters or how nitrate ions influence the physical properties of the absorbing disperse water medium.

The aim of the present study is to investigate the simultaneous interaction of water clusters with nitrate

ions and ozone molecules, and to establish the behavior of changes in spectral characteristics of disperse water systems, which result from such interactions.

### MOLECULAR-DYNAMICS MODEL

In the present work, a polarizable variant of the improved TIP4P model of water is employed [10]. A modification of the model fulfilled in [10] was connected with a considerable change in parameters of the Lennard-Jones (LJ) part of the potential; as a consequence, the coefficients with the terms describing repulsion and attraction were reduced by factors 2.5 and 2.9, respectively. Additionally, in this model, a negative charge was located at a point 0.0215 nm away from the oxygen nucleus instead of 0.015 nm as previously. This displacement allowed the permanent dipole moment of the water molecule to be corrected to 1.848 D, which corresponds to the experimental value in a gaseous phase.

Interactions between nitrate ions and between water and  $\text{NO}_3^-$  ions are thought of based on a polarizable model proposed in [11]. The parameters of the potential for  $\text{NO}_3^- - \text{H}_2\text{O}$  interactions were optimized so as to simulate the hydration energy and structural properties of a solvated nitrate ion. The molecular model of the  $\text{NO}_3^-$  ion represents a flat triangle with an N atom at the center and three O atoms at the corners. The angles between the bonds are identical and measure  $120^\circ$ , and the distance  $r_{\text{NO}} = 0.122$  nm. The partial electric charges of N and O atoms in the nitrate ion were determined as  $q_{\text{N}} = 0.5741e$ ,  $q_{\text{O}} = -0.5247e$  ( $e$  is the elementary charge). As a whole, the  $\text{NO}_3^-$  ion showed the electric charge  $q_{\text{NO}_3} = -1e$ . Quantum-mechanical calculations in the Hartree-Fock approximation determined the binding energy between the nitrate ion and water as 14.9 kcal/mol [12]. Electrostatic interactions between  $\text{O}_3$  molecules were determined by the charges  $q_{\text{cen}} = 0.19e$  and  $q_{\text{side}} = -0.095e$  [13] placed in the points of localization of central and side atoms, respectively. The angle  $\text{O}_{\text{side}} - \text{O}_{\text{cen}} - \text{O}_{\text{side}}$  in the ozone molecule is  $116.8^\circ$  [14]. The distance between the central and some of the edge atoms in the  $\text{O}_3$  molecule is  $r_{\text{OO}} = 0.1278$  nm.

A pair of the used atom-atomic potentials was treated as Lennard-Jones and Coulomb contributions. The parameters of the potential for the description of these interactions are given in the studies [11, 13]. Figure 1 shows atom-atomic LJ potentials  $\Phi(r)$  employed to describe the interactions between the nitrate ion and water molecules and ozone. The main difference between the potentials applied for the representation of  $\text{NO}_3^- - \text{H}_2\text{O}$  interactions (curves 1 and 2) and those characterizing the  $\text{NO}_3^- - \text{O}_3$  interactions

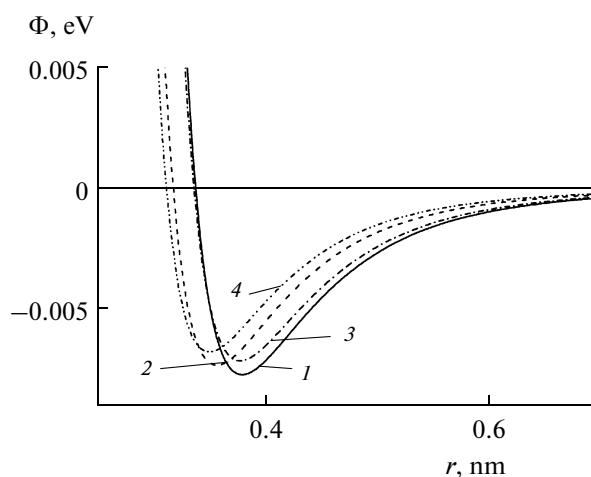


**Fig. 1.** Lennard-Jones potentials for the description of atom-atomic additive non-Coulomb interactions: (1)  $\text{N}-\text{O}_{\text{H}_2\text{O}}$ , (2)  $\text{O}_{\text{NO}_3}-\text{O}_{\text{H}_2\text{O}}$ , (3)  $\text{N}-\text{O}_{\text{O}_3}$ , and (4)  $\text{O}_{\text{NO}_3}-\text{O}_{\text{O}_3}$ .

(curves 3 and 4) is a shift in the repulsive branch and the potential well toward larger distances. The second distinction is a bit greater depth of the potential well when representing  $\text{NO}_3^- - \text{H}_2\text{O}$  interactions. In the functions  $\Phi(r)$  that describe interactions involving nitrate ions, deeper potential wells correspond to nitrogen. In molecular-dynamics calculations using the Stillinger-David polarization model [15], the potential energy  $U$  of a cluster  $(\text{H}_2\text{O})_{50}$  takes the value  $-24.25$  eV at  $T = 140$  K [16]. In the model presented herein, the  $U$  value for the  $(\text{H}_2\text{O})_{50}$  aggregate is  $-23.1$  eV at  $T = 237$  K.

Flexible models of molecules were considered. Molecule flexibility was achieved using the procedure devised within the framework of the Hamiltonian dynamics in [17, 18]. Let us consider the case of a diatomic molecule. Let atoms  $a$  and  $b$  be separated by the distance

$$Q = \|\mathbf{r}_a - \mathbf{r}_b\|,$$

where  $\mathbf{r}_a$  and  $\mathbf{r}_b$  are the vectors determining the positions of atoms. We denote the corresponding velocities by  $\mathbf{v}_a$  and  $\mathbf{v}_b$ , and the reduced mass is defined as

$$\mu = \frac{m_a m_b}{m_a + m_b}.$$

The size of a molecule represented by atoms  $a$  and  $b$  is determined by equalizing the total potential force  $\mathbf{f}(\mathbf{Q}) = -\frac{\partial \mathbf{r}}{\partial \mathbf{Q}} \nabla \Phi(\mathbf{r})$  and the centrifugal force  $-\mu Q \omega^2$ ; thus,

$$-\mu Q \omega^2 - \mathbf{f}(\mathbf{r}) \frac{\partial \mathbf{r}}{\partial \mathbf{Q}} = 0,$$

where  $\omega = \|\mathbf{v}_a - \mathbf{v}_b\|/Q$  is the angular velocity. From the condition of the minimum of the contribution

from each generalized coordinate to the potential energy  $U$ , we obtain

$$\frac{\partial}{\partial Q_i} H(\mathbf{r}, \mathbf{v}) = \frac{\partial}{\partial Q_i} \left( \frac{1}{2} \mu_i Q_i^2 \omega_i^2 + U(\mathbf{r}) \right) = 0.$$

This method is generalized to the molecules of any composition [19].

The simulation of interaction between the system  $6\text{O}_3 + (\text{H}_2\text{O})_{50}$  and  $\text{NO}_3^-$  ions began with the construction of a configuration composed of an equilibrium water cluster  $(\text{H}_2\text{O})_{50}$  and the surrounding ozone molecules. The initial equilibrium configurations of water clusters were obtained in separate molecular dynamics (MD) calculations, with the kinetic energy of molecules forming the cluster corresponding to a temperature of 237 K. The interaction of a water cluster with ozone molecules and nitrate ions was studied at the same temperature. Initially, the center of a free ozone molecule was located at a distance of 0.6 to 0.7 nm from the nearest center of the water molecule incorporated in the cluster. As this took place, the  $\text{O}_3$  molecule had a spontaneous orientation. As a result, each ozone molecule fell in the field of molecular interaction. The cutoff radius of molecular interactions in the model was 0.9 nm. Consequently,  $\text{O}_3$  molecules found themselves rather homogeneously distributed near the surface of the cluster  $(\text{H}_2\text{O})_{50}$ . Ions were brought to the system  $6\text{O}_3 + (\text{H}_2\text{O})_{50}$  in pairs and arranged on coordinate axes on different sides of the system at a distance of not less than 0.6 nm from any atom of the nearest molecule.

The molecular dynamics calculation was carried out at a time step of  $\Delta t = 0.2 \times 10^{-16}$  s. The calculation of spectral characteristics was begun after the system achieved an equilibrium state, which took a time of  $t_{ne} = 3 \times 10^5 \Delta t$  (6 ps). The  $(\text{O}_3)_6(\text{H}_2\text{O})_{50}$  cluster was also formed in  $\sim 3 \times 10^5 \Delta t$  time steps regardless of the presence of  $\text{NO}_3^-$  ions. The achievement of steady values of the total dipole moment by this aggregate, along with obtaining a stable distribution of bond lengths, evidenced the formation of the  $(\text{O}_3)_6(\text{H}_2\text{O})_{50}$  cluster. After the time  $t_{ne}$  expires, the dependence that the total energy of the system has on time starts fluctuating around the average value, which, along with the establishment of the Maxwellian velocity distribution, indicates that the equilibrium state is reached. From here on, we will take the beginning moment of the main calculation, that is, the moment when the system composed of water molecules, ozone, and nitrate ions achieves equilibrium, as  $t = 0$ . The duration of the main calculation comprised  $2.5 \times 10^6 \Delta t$  time steps.

The average bond length  $\langle L_b \rangle$  and the average number of bonds  $\langle n_b \rangle$  per unit water molecule was determined by construction of hybrid polyhedron (HP) in every thousand time steps. The HP is treated as an analogue of a Voronoy polyhedron (VP); i.e., it is a VP,

in whose center there is an O atom, and the neighbors forming faces are H atoms. The HPs were constructed for 25 oxygen atoms situated closer than others to the center of mass of the cluster. Thereby, the situations were excluded when it was impossible to construct a complete HP because there were no atoms in one of the half-spaces separated by some plane going through the center of mass of the HP. Of the nearest neighbors revealed by HPs, those were chosen for which the distance to them was not above 0.25 nm. This distance is close to the position of the first minimum in the partial function of radial distribution  $g_{\text{OH}}(r)$  of the  $(\text{O}_3)_6(\text{H}_2\text{O})_{50}$  cluster.

The Gear fourth-order method was employed to integrate the equations of motion of centers of mass of molecules [20]. This method is recommended to achieve greater calculation accuracy. This technique implies numerical schemes from the first to the sixth order of accuracy. A separate calculation showed that the restriction to a Taylor series of the fourth order, that is, using the time derivatives of coordinates up to the fourth order inclusive, gives an accuracy comparable to that in calculations of lower orders. However, when the order of this scheme is below four, it becomes less stable, which leads to a need for reducing the time step. Using the four-order scheme yields the optimum balance between the time step value and the computation time. In the MD method, the calculation error is determined principally by the systematic error, which depends on the integration scheme in use [21, 22]. The total calculation duration  $t_0$  ( $t_0 = 50$  ps) exceeded the characteristic time  $t_m$  ( $t_m \approx 10$  ps) of the fluctuation correlation of a network of hydrogen bonds in water [23]. The time  $t_m$  is controlled by a change in molecular orientations and distances, by breakage and recovery of hydrogen bonds, and by rotary motion. One may expect the calculation error for the autocorrelation functions [21, 22] and those obtained through the Fourier transform of their spectra to be not above  $(t_m/t_0)^{3/2} \approx 0.09$ . The error of determination of total energy fluctuations  $(\sqrt{\langle \Delta E^2 \rangle})/E \approx 0.095$  in the system formed by  $(\text{O}_3)_6(\text{H}_2\text{O})_{50}$  clusters involving from one to six  $\text{NO}_3^-$  anions is estimated by approximately the same value.

The analytical solution of motion equations for molecular rotation was accomplished using the Rodrigues–Hamilton parameters [24]; and the integration scheme of motion equations considering rotations corresponded to the approach proposed by Sonnenschein [25]. The calculations were performed with a quad-core Inter Core 2 Quad computer operating at a processor clock frequency of 2.83 GHz.

## DIELECTRIC PROPERTIES

Dielectric permittivity  $\epsilon(\omega)$  as a function of frequency  $\omega$  was represented by the complex value

$\varepsilon(\omega) = \varepsilon'(\omega) - i\varepsilon''(\omega)$ , which was calculated by the equation [26, 27]

$$\frac{\varepsilon(\omega) - 1}{\varepsilon_0 - 1} = -\int_0^{\infty} \exp(-i\omega t) \frac{dF}{dt} dt$$

$$= 1 - i\omega \int_0^{\infty} \exp(-i\omega t) F(t) dt,$$

where  $\varepsilon_0$  is the static dielectric permittivity and  $F(t)$  is the normalized autocorrelation function of the total dipole moment of a cluster:

$$F(t) = \frac{\langle \mathbf{d}_{\text{tot}}(t) \mathbf{d}_{\text{tot}}(0) \rangle}{\langle \mathbf{d}_{\text{tot}}^2 \rangle},$$

where

$$\mathbf{d}_{\text{tot}}(t) = \sum_{j=1}^N \mathbf{d}_j(t)$$

represents the sum of dipole moments of individual molecules.

Raman and IR spectra of clusters were calculated using the autocorrelation functions of polarizability and the dipole moment, respectively. The polar molecule is distinguished by the permanent (gas-phase) dipole moment  $\mathbf{d}_{i,0}$  and the polarization tensor  $\alpha_{i,0}$ . Interaction with neighboring molecules generates an induced dipole moment and polarizability of the molecule  $i$ . In the model, each molecule can be considered as a polarizable point dipole situated in the center of mass of the molecule. The dipole moment  $\mathbf{d}_i$  and polarizability  $\alpha_i$  of the molecule  $i$  are related owing to the interaction with surrounding molecules [28]

$$\mathbf{d}_i = \mathbf{d}_{i,0} + \alpha_{i,0} \sum_{j \neq i} \mathbf{T}_{ij} \mathbf{d}_j, \quad (1)$$

$$\alpha_i = \alpha_{i,0} + \alpha_{i,0} \sum_{j \neq i} \mathbf{T}_{ij} \alpha_j \quad (2)$$

Here  $\mathbf{T}_{ij}$  is the tensor of dipole–dipole interaction

$$\mathbf{T}_{ij} = \frac{1}{|r_{ij}|^3} (3\hat{\mathbf{r}}_{ij} \hat{\mathbf{r}}_{ij} - \mathbf{1}). \quad (3)$$

In Eq. 3,  $\hat{\mathbf{r}}_{ij}$  is a unit vector in the direction of  $\mathbf{r}_i - \mathbf{r}_j$ , where  $\mathbf{r}_i$  and  $\mathbf{r}_j$  are the positions of the centers of masses of the molecules  $i$  and  $j$ , and  $\mathbf{1}$  denotes a unit  $3 \times 3$  tensor. The anisotropic polarization gas-phase tensor  $\alpha_{xx,yy,zz} = \{1.495, 1.626, 1.286\} \text{ \AA}^3$  was used for the water molecule [29]. The  $\text{O}_3$  molecule shows a polarizability  $\alpha$  ( $2.85 \text{ \AA}^3$ ) above that of the water molecule ( $1.49 \text{ \AA}^3$ ) [14]. Isotropic polarizability of  $\text{NO}_3^-$  ions was set to the value  $4.47 \text{ \AA}^3$  [3].

Equations (1) and (2) for  $\mathbf{d}_i$  and  $\alpha_i$  can be solved by matrix inversion using the values  $\mathbf{d}_{i,0}$  and  $\alpha_{i,0}$  in the right-hand sides. Such a way of calculation gives the  $\mathbf{d}_i$  and  $\alpha_i$  values consistent with the corresponding parameters obtained by iterations [10]. If the dipole moments

of the molecules are determined, the absorption cross section of IR radiation is defined as [28]

$$\sigma(\omega) = \left( \frac{2}{\varepsilon_v c \hbar n} \right) \omega \text{th} \left( \frac{\hbar \omega}{2kT} \right) \text{Re} \int_0^{\infty} dt e^{i\omega t} \langle \mathbf{M}(t) \mathbf{M}(0) \rangle, \quad (4)$$

where  $n$  is the frequency-independent refractive index,  $\varepsilon_v$  is the vacuum dielectric permittivity, and  $c$  is the velocity of light.

In Eq. (4), the sum of vectors of individual molecular dipoles is defined as

$$\mathbf{M}(t) = \sum_{j=1}^N [\mathbf{d}_j(t) - \langle \mathbf{d}_j \rangle].$$

In the case of unpolarized light, the Raman spectra is given by the relation [28]

$$J(\omega) = \frac{\omega}{(\omega_L - \omega)^4} (1 - e^{-\hbar\omega/kT})$$

$$\times \text{Re} \int_0^{\infty} dt e^{i\omega t} \langle \Pi_{xz}(t) \Pi_{xz}(0) \rangle,$$

where

$$\Pi(t) = \sum_{j=1}^N [\alpha_j(t) - \langle \alpha_j \rangle].$$

$\omega_L$  is the frequency of an exciting laser,  $\Pi_{xz}$  represents the  $xz$  component of the  $\Pi(t)$  value, the  $x$  axis is directed along the molecular dipole, and  $xy$  is a molecular plane.

The reflection coefficient  $R$  is defined as the ratio between the average energy flux reflected from the surface and the incident flux. At normal incidence of a plane monochromatic wave, the reflection coefficient is described by the formula [30]

$$R = \frac{|\sqrt{\varepsilon_1} - \sqrt{\varepsilon_2}|^2}{|\sqrt{\varepsilon_1} + \sqrt{\varepsilon_2}|^2}. \quad (5)$$

It is supposed here that the incidence of a wave occurs from the transparent medium (medium 1) into a medium that can be either transparent or not, i.e., absorbing and scattering medium (medium 2). The indexes of the dielectric permittivity in Eq. 5 designate the medium.

The refractive index  $\eta$  and the absorption coefficient of the medium  $\xi$  are found from the equations [30]

$$\eta = \sqrt{\frac{\varepsilon' + \sqrt{\varepsilon'^2 + \varepsilon''^2}}{2}}, \quad \xi = \sqrt{\frac{-\varepsilon' + \sqrt{\varepsilon'^2 + \varepsilon''^2}}{2}}.$$

The coefficient  $\xi$  determines the rate of wave attenuation as it propagates through the medium. Let us denote the systems as I ( $\text{H}_2\text{O}$ ) $_n$ ,  $n = 10, 15, \dots, 50$ ; II ( $\text{H}_2\text{O}$ ) $_{50} + 6\text{O}_3 + i\text{NO}_3^-$ ,  $i = 1, 2, \dots, 6$ . The first system is composed of nine types of clusters, and the second one involves six types of them.

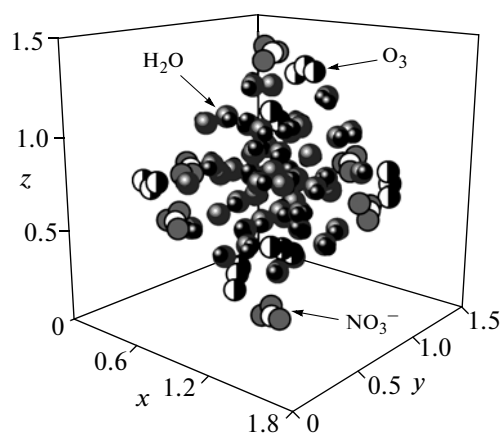


**Fig. 2.** Configuration of the cluster  $(\text{H}_2\text{O})_{50}(\text{O}_3)_6(\text{NO}_3^-)_6$  corresponding to the time point of 50 ps at  $T = 237$  K. Coordinates of molecules are given in nanometers.

### RESULTS OF CALCULATION

The configuration of a cluster  $(\text{H}_2\text{O})_{50}(\text{O}_3)_6(\text{NO}_3^-)_6$  formed by the time moment of 50 ps is shown in Fig. 2. It is seen that, by this point, nearly all  $\text{O}_3$  molecules and  $\text{NO}_3^-$  ions were absorbed by the water cluster, with the major portion of  $\text{O}_3$  molecules being located in the immediate vicinity of the  $\text{NO}_3^-$  ions. The  $\text{NO}_3^-$  ions are attached to ozone molecules mainly due to the formation of  $\text{N}\cdots\text{O}_{\text{cen}}$  bonds (here  $\text{O}_{\text{cen}}$  is the central atom in the ozone molecule), while  $\text{O}_{\text{NO}_3}\cdots\text{H}$  bonds are formed between them in close proximity to water molecules ( $\text{O}_{\text{NO}_3}$  is the oxygen atom in the nitrate ion). The newly formed cluster  $(\text{H}_2\text{O})_{50}(\text{O}_3)_6(\text{NO}_3^-)_6$  remains as a whole undivided construction during all calculations.

Figure 3a depicts a change in the number of  $\text{O}-\text{H}\cdots\text{O}$  bonds in clusters with respect to the number of nitrate ions adsorbed by them. It is seen that, when the first two ions are adsorbed, the number of bonds  $\langle n_b \rangle$  per molecule rises. However, the attachment of the third ion leads to a substantial drop in the  $\langle n_b \rangle$  value. Further increase in the number of ions in the cluster stabilizes the  $\langle n_b \rangle$  value at a level corresponding to the value of this parameter in the ozone-bearing water cluster with no  $\text{NO}_3^-$  ions present. Figure 3b illustrates a variation in the average  $\text{O}-\text{H}\cdots\text{O}$  bond length  $\langle L_b \rangle$  in the cluster as nitrate ions are added. One can see that a gain in the bond length is observed until the fourth ion is connected to the cluster. Further increase in the number of ions in the cluster leads to a weak reduction in the  $\langle L_b \rangle$  value. The initial increase in  $\langle L_b \rangle$  is associated with stretching out of the water carcass of the cluster by approaching  $\text{O}_3$  molecules and  $\text{NO}_3^-$  ions,

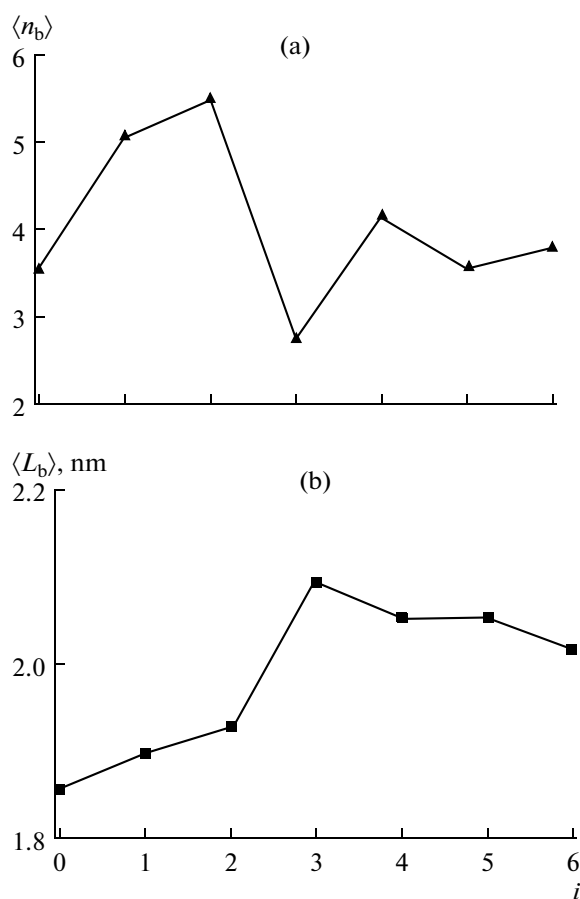


**Fig. 3.** Dependences that (a) the average number  $\langle n_b \rangle$  of bonds  $\text{O}-\text{H}\cdots\text{O}$  and (b) average lengths  $\langle L_b \rangle$  of these bonds have on the number of  $\text{NO}_3^-$  ions in system II ( $T = 237$  K).

and the subsequent decrease in the  $\langle L_b \rangle$  value is connected with repulsion of ions from the water nucleus. The approach of ions to the cluster is caused by the fact that hydrogen atoms of water molecules have an outward orientation at the cluster surface. The subsequent repulsion of ions from the water carcass results from the general prevalence of electrostatic repulsive forces over attractive forces in the system.

Figure 4 displays IR absorption spectra for systems I and II. The picture also presents experimental IR spectra of liquid water [31] and spectra of  $\text{O}_3$  [32] and  $\text{HNO}_3$  [33], which are present in the troposphere. The positions of the most intense bands in the IR spectrum for the water-cluster system (system I) and in the spectrum of liquid water ( $3389$  and  $3404$   $\text{cm}^{-1}$ ) correlate well. The presence of  $\text{NO}_3^-$  ions and ozone molecules in the cluster system shifts the most intense band to the region of lower frequencies. With increasing temperature of the water–ozone system containing  $\text{NO}_3^-$  anions, one can suppose that the inverse effect will emerge. When the temperature is increased to  $287$  K,

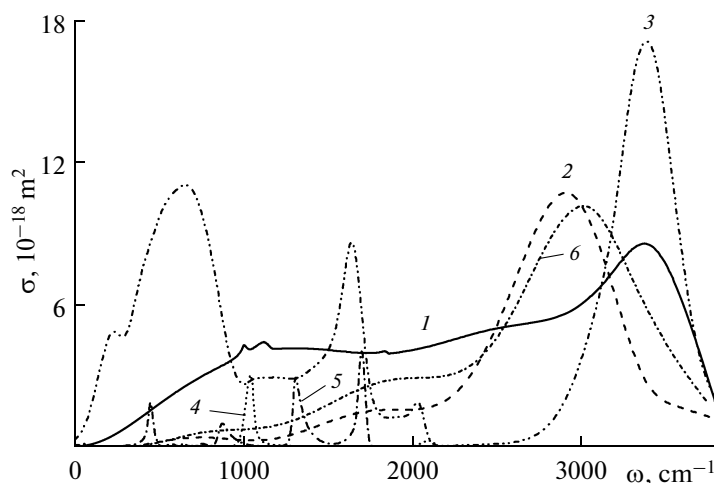


**Fig. 4.** IR absorption spectra of the systems: (1) I, (2) II (for 1 and 2  $T = 237$  K); (3) liquid water ( $T = 293$  K), the experiment [31]; (4, 5) stratospheric measurements of  $O_3$  [32] and  $HNO_3$  [33], respectively; (6) system II at  $T = 287$  K.

i.e., by 50 K, the most intense band in the spectrum of system II moves by  $103\text{ cm}^{-1}$  toward the region of high frequencies, and the intensity of this band decreases by 6.1%. A blue shift in absorption with rising temperature is caused by weakening of the hydrogen bonding and structural correlation. These factors are both determined by spectral diffusion [23], which essence lies in the fact that, with a rise in temperature, the transfer of quanta of OH-vibrations between the nearest oscillators is intensified. To put it differently, spectral diffusion is accounted for by the variation in vibration phases of modes typical of water. As a result of changes in the transfer of dipole vibrations, fluctuating forces appear, leading to weakening of hydrogen bonds and worsening of the structural correlation. This involves a rise in the intensity of the low-frequency portion of the IR spectrum (which finds itself to the left of the most intense band).

The most intense band in the IR spectrum of liquid water appears due to the superposition of three modes:  $\nu_1$  is symmetric stretching vibrations,  $\nu_3$  is antisymmetric stretching vibrations, and the overtone of a mode  $\nu_2$  is deformation vibrations (bending of covalent bonds). The mode  $\nu_2$  is responsible for the emergence of a band at  $1644\text{ cm}^{-1}$ . The band at  $690\text{ cm}^{-1}$  is formed owing to librations determined by restrictions imposed by hydrogen bonding. The weak band at  $200\text{ cm}^{-1}$  is associated with translation vibrations, including stretching of the  $O-H\cdots O$  hydrogen bond and its bending. At the IR spectrum of the water-cluster system I, a blue shift of the libration mode by  $\sim 380\text{ cm}^{-1}$  relative to the corresponding band in the IR spectrum of bulk water is observed. This band of system I is positioned between the positions of the second and the third peaks in the IR spectrum of stratospheric  $HNO_3$ .

The IR spectrum of system II at  $T = 237$  K shows three broad bands. The first one, of weak intensity, is

localized at  $748\text{ cm}^{-1}$ , the second, more intensive, band finds itself at  $1842\text{ cm}^{-1}$ , and the third, most intensive, one is located around  $2936\text{ cm}^{-1}$ . The position of the first band agrees with quantum-mechanical calculations of localization of the mode of deformation vibrations ( $720\text{ cm}^{-1}$ ) in the complex  $NO_3^-/H_2O$  [12]. The second band occurs in the vicinity of the doubled frequency ( $1993\text{ cm}^{-1}$ ) of the mode of anti-symmetric vibrations of ozone molecules, which was found empirically in the study [34]. The third band for the water-cluster system containing  $O_3$  molecules and  $NO_3^-$  ions has a red shift relative to the position ( $3389\text{ cm}^{-1}$ ) of the most intense band in the IR spectrum of system I. The absorption band at  $\sim 1058\text{ cm}^{-1}$  for stratospheric ozone occurs owing to the superposition of modes of symmetric and antisymmetric stretching vibrations ( $1063\text{ cm}^{-1}$ ) in ozone [34].

The work [6] showed that the absorption by  $(H_2O)_{50}$  clusters of both molecular and monatomic oxygen yields a reduction in the integral intensity  $I_{tot}$  of the IR absorption spectrum by a factor of 1.5–2. In the course of the study, IR absorption spectra were calculated for the disperse water system III with nitrate ions  $(H_2O)_{50} + 6O_2 + iNO_3^-$ , in which clusters adsorbed oxygen molecules rather than ozone molecules. The value  $I_{tot}$  for system II (with ozone) appeared to be 1.6 times lower than that for system III (with oxygen). The capture of ozone by water clusters significantly decreases the ability of the disperse water system to absorb IR radiation.

The Raman spectra of systems I and II are represented by a great number of well-resolved peaks (Fig. 5). The three most intense peaks of system II fall on the frequencies of 938, 1941, and  $3125\text{ cm}^{-1}$ . The most intense band in the Raman spectrum of disperse water system I is localized at  $3040\text{ cm}^{-1}$ . The Raman

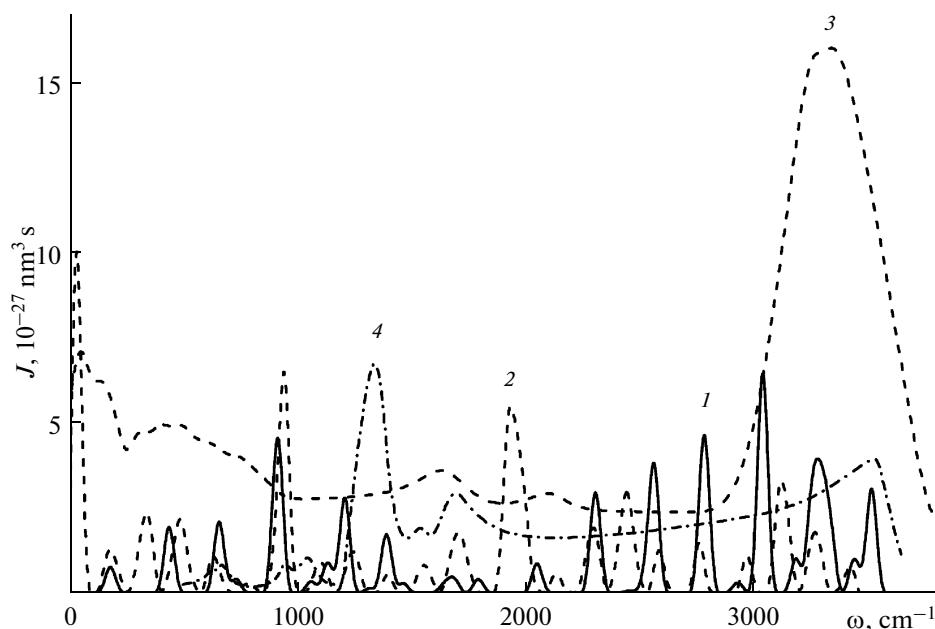


**Fig. 5.** Raman spectra for the systems: (1) I, (2) II (for 1 and 2  $T = 237$  K); (3) liquid water ( $T = 293$  K), the experiment [35]; (4) Raman spectrum of the complexes  $\text{NO}_3^-$  and  $\text{N}_2\text{O}_4$  in a 78% water solution of  $\text{HNO}_3$  [36] (for 3 and 4  $T = 293$  K).

spectrum of liquid water [35] shows the most intense band at  $3337\text{ cm}^{-1}$ , and the Raman spectrum of complexes  $\text{NO}_3^-$ ,  $\text{N}_2\text{O}_4$  in a 78% water solution of  $\text{HNO}_3$  [36] has a band at  $1350\text{ cm}^{-1}$ . Characteristic vibrations in liquid water occur with average intensities of  $200\text{ cm}^{-1}$  and  $686\text{ cm}^{-1}$ . With allowance for anharmonicity of vibrations, one can expect that summation of these modes will result in the appearance of a band at the Raman spectrum localized around a frequency of  $900\text{ cm}^{-1}$ . The intensity of the band at  $938\text{ cm}^{-1}$  in the Raman spectrum of system II grew with respect to the corresponding characteristic in the spectrum of system I (a band at  $917\text{ cm}^{-1}$ ). This amplification occurs thanks to the influence of  $\text{NO}_3^-$  ions. Hydrated  $\text{NO}_3^-$  ions have a strong band in the Raman spectrum at  $1049\text{ cm}^{-1}$  [36]. A band at  $1941\text{ cm}^{-1}$  at the  $J$ -spectrum of the system II, on the one hand, can be considered as an analogue of the mode ( $2125\text{ cm}^{-1}$ ) in liquid water resulting from the combination between the mode of deformation vibrations  $\nu_2$  and libration modes. On the other hand, ozone modes are represented as combinations of frequencies ( $2\nu_3$ ,  $\nu_1 + \nu_3$ , and  $2\nu_1$ ) in the range of  $1993$ – $2143\text{ cm}^{-1}$ . Since the Raman spectrum of system I shows a very weak replica at  $2048\text{ cm}^{-1}$ , the emergence of a strong band in the vicinity of this frequency in the Raman spectrum of system II can be attributed to the determining influence of ozone. The peaks at high frequencies ( $3040$  and  $3125\text{ cm}^{-1}$ ) are likely to be caused by overtones of the mode of intense longitudinal vibrations, which appears in liquid water at  $273\text{ K}$  in the form of the most

intense band at  $686\text{ cm}^{-1}$ , in combination with the mode of longitudinal vibrations at a frequency of  $395\text{ cm}^{-1}$  (the total frequency amounts to  $3139\text{ cm}^{-1}$ ).

Figure 6 depicts the frequency spectra of the reflection coefficient of disperse water systems I and II. The maximum of the  $R$ -spectrum of the system (I) of pure-water clusters falls on a frequency of  $1041\text{ cm}^{-1}$ , and that of the spectrum of the system (II) adsorbing ozone and nitrate ions localizes at  $2882\text{ cm}^{-1}$ . The disperse water system I has the average (in frequency) IR reflection coefficient of  $\bar{R} = 0.35$ , while the same parameter for system II is  $0.94$ . The spectrum  $R(\omega)$  for system I is fitted by a curve with a single pronounced peak, and the corresponding spectrum for system II is approximated by a frequency dependence with three peaks. Thus, homogeneous deposition of ozone molecules and nitrate ions onto the surface of  $(\text{H}_2\text{O})_{50}$  clusters produces high-efficiency reflection of IR radiation by the cluster system.

The optical properties of small particles are usually determined by the refractive index  $\eta$  and the absorption coefficient  $\xi$ . The refractive index is a measure of the substance's ability to deflect light rays falling on it. The index  $\eta$  does not depend on the incidence angle of a light wave and is the ratio between the velocity of light in a vacuum and the phase velocity in the medium. Propagation of light through media is a rather complicated phenomenon. Light waves enter into interactions with atoms of a substance, exciting them, and, therewith, generating secondary light, i.e., the light produced by radiation from the medium

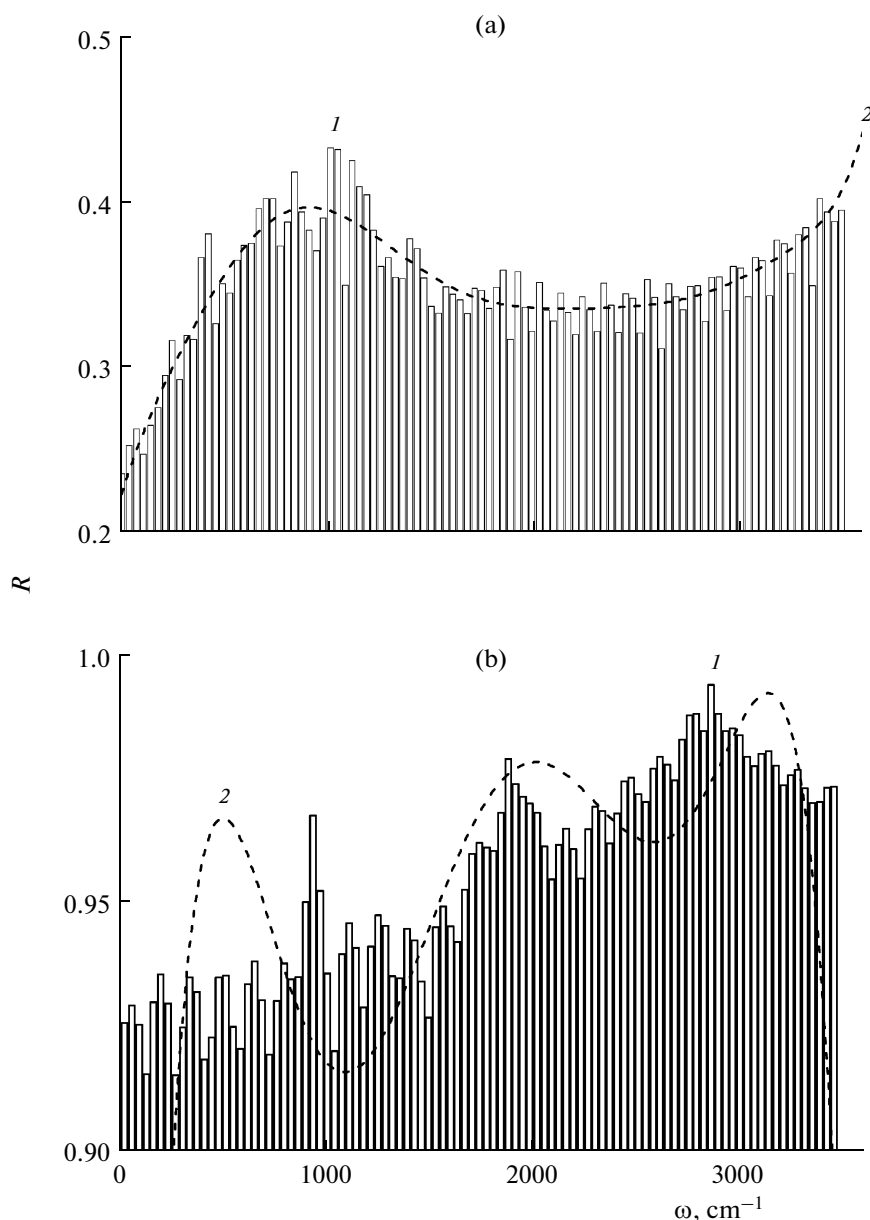


**Fig. 6.** Reflection coefficients  $R$  of IR radiation for the cluster systems at  $T = 237$  K: (a) system I, (b) system II; (1) MD calculations, (2) approximation of the calculated dependence by the polynomial  $R(\omega)$  of the sixth order.

itself. Exhibiting the same phase characteristics as the incident light, it is summed up with the latter, which leads to a change in phase velocities and, thus, to dispersion. In cases of normal dispersion of light, the refractive index  $\eta$  is above unity. Consequently, dissipation or growth in the energy of the wave field takes place, which are described using the absorption coefficient  $\xi$ .

The calculated optical constants  $\xi$  and  $\eta$  for systems I and II are shown in Fig. 7 along with the corresponding experimental values of these parameters for liquid water [37] and nitric acid [38]. One can see that, in the entire frequency range, the  $\xi$  value for the sys-

tem of pure-water clusters is above that of the system  $(\text{H}_2\text{O})_{50} + 6\text{O}_3 + i\text{NO}_3^-$ . The coefficient  $\xi$  determines the rate of wave attenuation as it propagates. Therefore, the rates of wave attenuation for all considered frequencies are higher in system I than those in system II. The average value of coefficient  $\xi$  with respect to frequency for system I amounted to 0.72, and, for system II, it was 0.53. By contrast, the refractive index  $\eta$  for system II was above that for system I; that is, system II is more dense optically than system I. In addition, the refractive index of system II is weakly dependent on frequency. Almost everywhere throughout the spectrum portion at frequencies  $\omega > 445$   $\text{cm}^{-1}$ , the

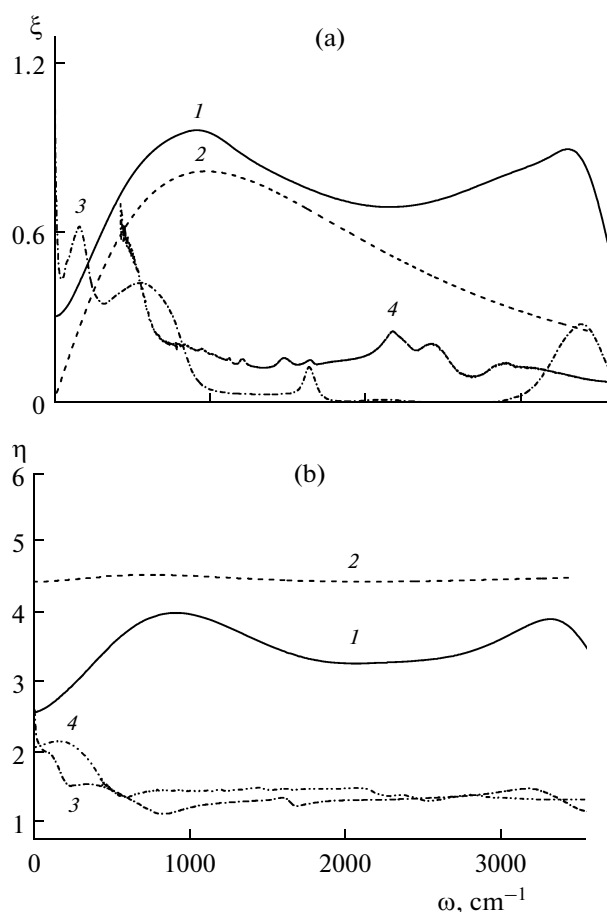


**Fig. 7.** Absorption coefficient of the medium (a) and refractive index (b) for the systems: (1) I, (2) II (for 1 and 2  $T = 237$  K), (3) experimental values of  $\xi$  and  $\eta$  ( $T = 293$ ) for liquid water [37], (4) experimental values of  $\xi$  and  $\eta$  for nitric acid ( $\text{HNO}_3$ ) [38].

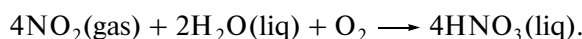
coefficient  $\xi$  of cluster systems takes higher values rather than those of liquid water and nitric acid, and the index  $\eta$  for cluster systems is above the corresponding parameters of liquid  $\text{H}_2\text{O}$  and  $\text{HNO}_3$  at all studied frequencies. Thus, a significant decrease in the rate of propagation of IR radiation takes place in cluster systems.

## CONCLUSIONS

In the present work, the mechanism of adsorption of nitrate ions and ozone by water clusters is investigated. The initial orientation of surface water molecules in a cluster with hydrogen directed outwards produced an attractive force for  $\text{NO}_3^-$  ions. Since the initial distances between  $\text{NO}_3^-$  ions were more than two times above those from ions to hydrogen atoms, ions moved toward the cluster thanks to Coulomb attraction. Next, a heterocluster formed due to Lennard-Jones interactions. Ozone molecules bearing small dis-

tributed electric charges did not hinder the attachment of ions to the surface of the water cluster. Polarization interaction also created a stabilizing effect. Eventually, in a time interval of 50 ps, negatively charged clusters with a water core were observed, with  $\text{NO}_3^-$  ions and ozone molecules situated at their surface.

Ozone is a very powerful oxidizer, much more powerful than oxygen. Therefore, the following processes should actually take place further at the surface of a cluster that adsorbed ozone and  $\text{NO}_3^-$  ions. At the high concentrations observed, ozone decomposes into ordinary diatomic and monatomic oxygen. Under atmospheric conditions its half-life is approximately 30 min. Monatomic oxygen forms  $\text{NO}_2$  and  $\text{O}_2$  reacting with  $\text{NO}_3^-$ . Ultimately, nitrogen dioxide enters into a reaction with water and oxygen giving nitric acid:



A portion of  $\text{NO}_2$  can stay on the surface of the cluster formed by a water solution of nitric acid.

Thus, the action of nitrate ions is similar to that produced by  $\text{Cl}^-$  and  $\text{Br}^-$  ions destroying ozone at the water surface. Adsorption of  $\text{NO}_3^-$  ions and ozone molecules by water clusters leads to a significant drop in the absorbing ability of the disperse water system. Water clusters with  $\text{NO}_3^-$  and  $\text{O}_3$  deposited on their surfaces reflect a major portion of the incoming IR radiation. Therefore, a smaller portion of the IR is trapped within the atmosphere. The greenhouse effect is reduced because of both lowering IR absorption by clusters and destroying ozone at their surfaces.

## ACKNOWLEDGMENTS

This study was supported by the Russian Foundation for Basic Research, project no. 08-08-00136-a.

## REFERENCES

1. Golobokova, L.P., Latysheva, I.V., Mordvinov, V.I., Khodzher, T.V., Obolkin, V.A., and Potemkin, V.L., *Atmos. Oceanic Opt.*, 2005, vol. 18, no. 8, p. 616.
2. Foster, K.L., Plastringe, R.A., Bottenheim, J.W., Shepson, P.B., Finlayson-Pitts, B.J., and Spicer, C.W., *Science* (London), 2001, vol. 291, p. 471.
3. Salvador, P., Curtis, J.E., Tobias, D.J., and Jungwirth, P., *Phys. Chem. Chem. Phys.*, 2003, vol. 5, p. 3752.
4. Galashev, A.E., *High Temp.*, 2010, vol. 48, no. 4, p. 518.
5. Galashev, A.E., Rakhmanova, O.R., and Novruzova, O.A., *High Temp.*, 2011, vol. 49, no. 2, p. 193.
6. Novruzova, O.A. and Galashev, A.E., *High Temp.*, 2008, vol. 46, no. 1, p. 60.
7. Galashev, A.E., Rakhmanova, O.R., and Chukanov, V.N., *High Temp.*, 2009, vol. 47, no. 3, p. 342.
8. Galashev, A.E. and Rakhmanova, O.R., *Russ. J. Phys. Chem. A*, 2010, vol. 84, no. 8, p. 1364.

9. Galashev, A.Y., *Int. J. Energy, Environ. Econ.*, 2010, vol. 19, no. 6, p. 121.
10. Dang, L.X. and Chang, T.-M., *J. Chem. Phys.*, 1997, vol. 106, p. 8149.
11. Dang, L.X., Chang, T.-M., Roeselova, M., Garrett, B.C., and Tobias, D.J., *J. Chem. Phys.*, 2006, vol. 124, p. 066101.
12. Shem, M., Xie, Y., Schaefer, H.F., and Deakne, C.A., *Chem. Phys.*, 1991, vol. 151, p. 187.
13. Hunt, S.W., Roeselová, M., Wang, W., Wingen, L.M., Knipping, E.M., Tobias, D.J., Dabdub, D., and Finlayson-Pitts, B.J., *J. Phys. Chem. A*, 2004, vol. 108, p. 11559.
14. *Spravochnik khimika* (A Chemist's Handbook), Nikol'skii, B.P., Ed., Leningrad: Khimiya, 1966, vol. 1.
15. Stillinger, F.H. and David, C.W., *J. Chem. Phys.*, 1978, vol. 69, p. 1473.
16. Vostrikov, A.A., Dubov, D.Yu., and Drozdov, S.V., *Tech. Phys. Lett.*, 2008, vol. 34, no. 3, p. 221.
17. Lemberg, H.L. and Stillinger, F.H., *J. Chem. Phys.*, 1975, vol. 62, p. 1677.
18. Rahman, A., Stillinger, F.H., and Lemberg, H.L., *J. Chem. Phys.*, 1975, vol. 63, p. 5223.
19. Saint-Martin, H., Hess, B., and Berendsen, H.J.C., *J. Chem. Phys.*, 2004, vol. 120, p. 11133.
20. Haile, J.M., *Molecular Dynamics Simulation: Elementary Methods*, New York: Wiley, 1992.
21. Norman, G.E. and Stegailov, V.V., *JETP*, 2001, vol. 92, no. 5, p. 879.
22. Kuksin, A.Y., Morozov, I.V., Norman, G.E., Stegailov, V.V., and Valuev, I.A., *Mol. Simul.*, 2005, vol. 31, p. 1005.
23. Kraemer, D., Cowan, M.L., Paarmann, A., Huse, N., Nibbering, E.T.J., Elsaesser, T., and Miller, R.J.D., *Proc. Natl. Acad. Sci. USA*, 2008, vol. 105, p. 437.
24. Koshlyakov, V.N., *Zadachi dinamiki tverdogo tela i prikladnoi teorii giroskopov* (Problems in the Dynamics of a Solid Body and the Applied Theory of Gyroscopes), Moscow: Nauka, 1985.
25. Sonnenschein, R., *J. Comput. Phys.*, 1985, vol. 59, p. 347.
26. Bresme, F., *J. Chem. Phys.*, 2001, vol. 115, p. 7564.
27. Neumann, M., *J. Chem. Phys.*, 1985, vol. 82, p. 5663.
28. Bosma, W.B., Fried, L.E., and Mukamel, S., *J. Chem. Phys.*, 1993, vol. 98, p. 4413.
29. Huiszoon, C., *Mol. Phys.*, 1986, vol. 58, p. 865.
30. Landau, L.D. and Lifshitz, E.M., *Course of Theoretical Physics, Volume 8: Electrodynamics of Continuous Media*, Oxford: Butterworth-Heinemann, 1984.
31. Goggin, P.L. and Carr, C., in *Water and Aqueous Solutions*, Neilson, G.W. and Enderby, J.E., Eds., Bristol: Adam Hilger, 1986, vol. 37, p. 149.
32. Wagner, G., Birk, M., Schreier, F., and Flaud, J.-M., *J. Geophys. Res.*, 2002, vol. 107, p. 22.
33. Goldman, A., Murcray, F.J., Blatherwick, R.D., Kosters, J.J., Murcray, D.G., Rinsland, C.P., Flaud, J.-M., and Camy-Peyret, C., *J. Geophys. Res.*, 1992, vol. 97, p. 2561.
34. Rinsland, C.P., Flaud, J.-M., Perrin, A., Birk, M., Wagner, G., Goldman, A., Barbe, A., De Backer-Barilly, M.-R., Mikhailenko, S.N., Tyuterev, V.I.G., Smith, M.A.H., Malathy Devi, V., Benner, D.C., Schreier, F., Chance, K.V., Orphal, J., and Stephen, T.M., *J. Quant. Spectrosc. Radiat. Transfer*, 2003, vol. 82, p. 207.
35. Murphy, W.F., *J. Chem. Phys.*, 1977, vol. 67, p. 5877.
36. Kamboures, M.A., van der Veer, W., Gerber, R.B., and Phillips, L.F., *Phys. Chem. Chem. Phys.*, 2008, vol. 10, p. 4748.
37. Downing, H.D. and Williams, D., *J. Geophys. Res.*, 1975, vol. 80, p. 1656.
38. Biermann, U.M., Luo, B.P., and Peter, Th., *J. Phys. Chem. A*, 2000, vol. 104, p. 783.